The 3.2 Å Resolution Structure of a Receptor:CheA:CheW Signaling Complex Defines Overlapping Binding Sites and Key Residue Interactions within Bacterial Chemosensory Arrays

ARTICLE *in* BIOCHEMISTRY · MAY 2013

Impact Factor: 3.02 · DOI: 10.1021/bi400383e · Source: PubMed

8 AUTHORS, INCLUDING:

Xiaoxiao Li
Cornell University
4 PUBLICATIONS **93** CITATIONS
SEE PROFILE

Aaron D Fleetwood
University of Tennessee
2 PUBLICATIONS **21** CITATIONS
SEE PROFILE

Davi R Ortega
California Institute of Technology
15 PUBLICATIONS **266** CITATIONS
SEE PROFILE

Igor Zhulin
Oak Ridge National Laboratory
87 PUBLICATIONS **5,792** CITATIONS
SEE PROFILE

BIOCHEMISTRY
including biophysical chemistry & molecular biology

Article

pubs.acs.org/biochemistry

The 3.2 Å Resolution Structure of a Receptor:CheA:CheW Signaling Complex Defines Overlapping Binding Sites and Key Residue Interactions within Bacterial Chemosensory Arrays

Xiaoxiao Li,[†] Aaron D. Fleetwood,[‡] Camille Bayas,[†] Alexandrine M. Bilwes,[†] Davi R. Ortega,[‡] Joseph J. Falke,[⊥] Igor B. Zhulin,*[,‡] and Brian R. Crane*[,†]

[†]Department of Chemistry and Chemical Biology, Cornell University, Ithaca, New York 14853, United States

[‡]Computer Science and Mathematics Division, Oak Ridge National Laboratory, Oak Ridge, Tennessee 37831, United States, and Department of Microbiology, University of Tennessee, Knoxville, Tennessee 37996, United States

[⊥]Department of Chemistry and Biochemistry and the Molecular Biophysics Program, University of Colorado, Boulder Colorado 80309-0215, United States

Supporting Information

ABSTRACT: Bacterial chemosensory arrays are composed of extended networks of chemoreceptors (also known as methyl-accepting chemotaxis proteins, MCPs), the histidine kinase CheA, and the adaptor protein CheW. Models of these arrays have been developed from cryoelectron microscopy, crystal structures of binary and ternary complexes, NMR spectroscopy, mutational, data and biochemical studies. A new 3.2 Å resolution crystal structure of a *Thermotoga maritima* MCP protein interaction region in complex with the CheA kinase-regulatory module (P4−P5) and adaptor protein CheW provides sufficient detail to define residue contacts at the interfaces formed among the three proteins. As in a previous 4.5 Å resolution structure, CheA-P5 and CheW interact through conserved hydrophobic surfaces at the ends of their β-barrels to form pseudo 6-fold symmetric rings in which the two proteins alternate around the circumference. The interface between P5 subdomain 1 and CheW subdomain 2 was anticipated from previous studies, whereas the related interface between CheW subdomain 1 and P5 subdomain 2 has only been observed in these ring assemblies. The receptor forms an unexpected structure in that the helical hairpin tip of each subunit has "unzipped" into a continuous α-helix; four such helices associate into a bundle, and the tetramers bridge adjacent P5-CheW rings in the lattice through interactions with both P5 and CheW. P5 and CheW each bind a receptor helix with a groove of conserved hydrophobic residues between subdomains 1 and 2. P5 binds the receptor helix N-terminal to the tip region (lower site), whereas CheW binds the same helix with inverted polarity near the bundle end (upper site). Sequence comparisons among different evolutionary classes of chemotaxis proteins show that the binding partners undergo correlated changes at key residue positions that involve the lower site. Such evolutionary analyses argue that both CheW and P5 bind to the receptor tip at overlapping positions. Computational genomics further reveal that two distinct CheW proteins in Thermotogae utilize the analogous recognition motifs to couple different receptor classes to the same CheA kinase. Important residues for function previously identified by mutagenesis, chemical modification and biophysical approaches also map to these same interfaces. Thus, although the native CheW−receptor interaction is not observed in the present crystal structure, the bioinformatics and previous data predict key features of this interface. The companion study of the P5-receptor interface in native arrays (accompanying paper Piasta et al. (2013) *Biochemistry*, DOI: 10.1021/bi400385c) shows that, despite the non-native receptor fold in the present crystal structure, the local helix-in-groove contacts of the crystallographic P5-receptor interaction are present in native arrays and are essential for receptor regulation of kinase activity.

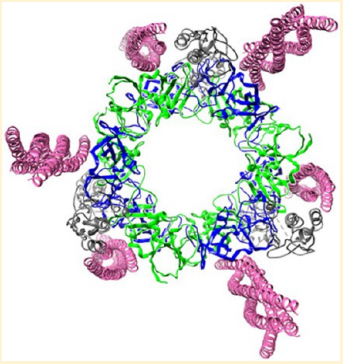

Bacterial chemotaxis,[1] the tendency of bacteria to swim toward attractants and away from repellants, has long served as a model system for understanding transmembrane signaling, motility, and cellular behavior.[2−4] Moreover, the underlying sensory pathways of chemotaxis are essential for the infectivity of many prokaryotic pathogens such as *Helicobacter pylori* (gastric ulcers and stomach cancers),[5−8] *Vibrio cholerae* (cholera),[8−10] and several types of pathogenic Spirochetes (lyme diseases, dental disease, syphilis).[11−13] It has become increasingly apparent that the receptors responsible for binding chemoattractants form extended, ordered structures in the cytoplasmic membranes of cells. These chemosensory arrays are primarily composed of the chemoreceptors themselves, also called methyl-accepting chemotaxis proteins (MCPs), the histidine kinase CheA, and the adaptor protein CheW.[14−18] Cryo-electron microscopy (cryoEM) has revealed a hexagonal arrangement

Received: March 25, 2013
Revised: May 9, 2013
Published: May 13, 2013

for these receptor clusters[19−24] that is based upon a conserved trimeric assembly of chemoreceptors[3] found in species that range from proteobacteria to Thermotogae.[25]

Although sensing domains differ among MCPs, the receptors all have a similar construction and are exemplified by the four *Escherichia coli* chemoreceptors, Tar, Tsr, Trg, and Tap.[3,26−28] Dimeric MCPs span the membrane with four helices (TM1, TM2, TM1′, and TM2′), bind ligands through a variable amino-terminal extracellular domain, and interact with cellular components through a well-conserved carboxy-terminal cytoplasmic domain (MCP_C). MCP_C is linked to TM2 by a short cytoplasmic HAMP domain that is key to transducing signals across the membrane.[29−32] Each MCP_C subunit folds as two long antiparallel helices that dimerize into a four-helix bundle.[33−35] The region most distal to the membrane (the tip of the bundle) known also as the protein interaction region (PIR) or the kinase control module (KCM) interacts with CheA through CheW. In the so-called "adaptation region", glutamate residues ∼140−195 Å away from the receptor tip undergo reversible methylation/demethylation (by CheR and CheB or/and CheD, respectively) to tune receptor activation of CheA.[36−39] Regulation of the CheB methyl-esterase activity by CheA allows the system sensitivity to adjust to conditions and thereby generates feedback control (also known as adaptation).

The histidine kinase CheA complexes with receptors and transduces ligand binding events into initiation of an intracellular phosphorelay that ends by regulating rotation of the flagellar motor.[40−42] CheA is a dimer with each subunit containing five separate functional units (P1 to P5), strung together as distinct domains over the length of the polypeptide.[43−49] P1 contains the substrate histidine autophosphorylated by the kinase domain (P4). P2 docks CheY for phosphotransfer from P1. The last three domains (P3−P4−P5) comprise dimerization, kinase (ATP binding), and receptor-coupling modules, respectively, and their structures have been determined together for *Thermotoga maritima* CheA (CheAΔ289).[43]

The final core component of the signaling ternary complex is the adaptor protein CheW.[50,51] CheW has the same tandem SH3-domain-like fold as the CheA P5 regulatory domain and conserves two intertwined five-stranded β-barrels (designated subdomains 1 and 2).[43,52] The P3-proximal barrel of P5 (subdomain 1) binds CheW through a pseudosymmetric contact that involves conserved hydrophobic residues on each domain.[34,52−56] Early observations showed that CheW is required for kinase activation,[57,58] and more recent studies suggest that CheW and CheA P5 may compete for binding receptors.[59,60]

We produced a model of the receptor:CheA:CheW cytoplasmic ternary complex by application of site-specific spin labeling with nitroxides and pulsed-dipolar electron spin resonance (ESR) spectroscopy to soluble complexes of MCP_C, CheA and CheW from *T. maritima*.[61] Overall, the data revealed that the receptor tip binds CheW but also interacts between the P4 and P5 domains of CheA. The ESR structure is surprisingly asymmetric with the receptor stalk aligning along the CheA dimerization domain and the P1 substrate and P4 kinase domains projected away from the receptor tips,[61] as proposed by a model based on chemical modification studies of the complex.[54]

More recently, we determined the crystallographic structure of a complex between CheA (P4−P5):CheW and a truncated MCP_C from the *T. maritima* soluble receptor Tm14 (PDB code 3UR1[62]). This structure was fit to electron density from cryoEM maps of native receptor arrays in the cytoplasmic membranes of cells.[62] The original crystals diffracted to only 4.5 Å resolution, but their high solvent content enabled placement of the proteins and domains. The receptor PIR interacts with the surface of CheW expected from our PDS studies,[61] but CheA P5 and CheW form rings of pseudohexagonal symmetry that are consistent with the honeycomb receptor lattice observed by cryoEM and predicted by the domain arrangements found by PDS.[61,62] The combined methods describe a P6 lattice symmetry for the receptor arrays where rings of CheA and CheW associate receptor trimers-of-dimers into a hexagonal network and the P4 kinase domains suspend below the CheW-P5 rings. We have modeled and refined crystallographic structures against the cryoEM data and confirmed that the crystallographic assembly states are consistent with the native arrays within the resolution range of 20−30 Å.[62] NMR studies verified interfaces implied by the extended structure,[63,64] and a very similar model has been subsequently published based on independent cryoEM data.[24]

Despite these advances, the low resolution of the ternary complex structure prevents a detailed description of the molecular interactions within the chemosensory arrays. Indeed, electron density for side chains could not be resolved in the maps, and although the topology of CheA and CheW allow for a largely unambiguous placing of their secondary structure, the register and rotational orientation of the receptor helices was uncertain.[62] Furthermore, the interaction between the receptor tip and the CheA-P5 domain could only be modeled on the CheW receptor interaction because in the crystals, P5 interacts with the receptor at a position that was only assumed to mimic the native association. Greater structural detail is necessary to not only refine the overall architecture of the arrays, but also understand the mechanism for switching activity states. With the aim of improving the ternary complex crystals, we have reengineered the receptor fragments by perturbing helix termini involved in lattice contacts. One of these altered fragments consistently produced crystals that diffracted to better than 3.5 Å resolution. The resulting higher resolution structure confirms the P5:CheW rings of the previous structure, but the receptor itself displays an unusual unzipped conformation in which a tetrameric 4-helix bundle associates the CheA P5 domains and CheW. This unzipped structure has not been observed in native arrays and is believed to be a non-native feature. However, evolutionary analysis of sequence conservation and mutation patterns suggests that the contacts among the receptor, CheA, and CheW displayed by the structure are relevant to the native chemosensory system. The companion paper directly confirms the predicted receptor-P5 interface is present in the native, membrane-bound array and shows the intact interface is essential for receptor regulation of CheA activity.[65]

EXPERIMENTAL PROCEDURES

Constructs of *T. maritima* $Tm14_S$ with altered termini (residues 107−192, 107−193, 107−194, 106−191, 106−192) compared to those that produced the previous 3UR1 structure (107−191) were PCR cloned into vector pET28a (Novagen) and expressed with an N-terminal $histidine_6$ tag in *E. coli* strain BL21 (RIL DE3) (Novagen) after induction with IPTG at 18 °C and overnight growth for 21 h. The Tm14s fragments were purified first with Ni-NTA chromatography, followed by overnight thrombin digestion, and then size-exclusion chromatography (Superdex 75 Hi-load FPLC column in 50 mM NaCl, 100 mM Tris pH 7.5, 10% glycerol). *T. maritima* CheW and CheA Δ354 (P4P5 domain, residues 355−671) were expressed and purified as described previously.[34]

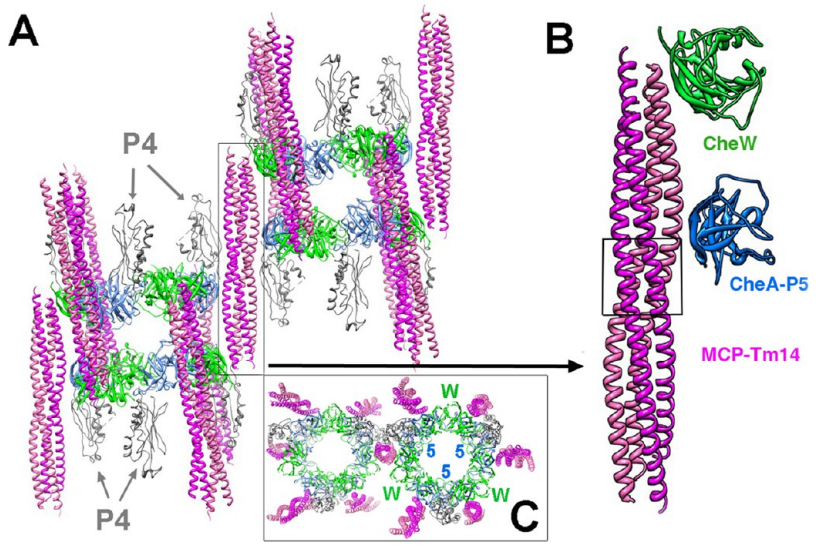

Figure 1. Molecular composition of the 3.2 Å resolution ternary complex crystals. (A) Molecular interactions generated by the *R*32 crystal symmetry. CheW (green) and the CheA P5 domain (blue) form rings of 3-fold symmetry, with the two proteins alternating around the circumference. The P5-CheW rings are held together by extended 4-helix bundles formed by the $Tm14_S$ receptor (pink and purple). Four $Tm14_S$ subunits have unzipped into continuous helices and associate into a tetrameric 4 helix bundle; each bundle binds two P5 domains near its center (lower site) and two CheW domains at its periphery (upper site). If the pink helices were joined at the middle of the bundle, and the purple helices were similarly joined, they would produce end-to-end MCP hairpin tips as reported in the previous 4.5 Å resolution structure (see Figure 2). $Tm14_S$ tetramers interact with every P5 or CheW domain around the ring, alternating up and down. The CheA P4 domains (gray) project in large solvent channels above and below the rings, although their electron density is not well-defined. (B) Close-up of the $Tm14_S$ tetramer and its interaction with one P5 domain near its center and one CheW at its end. The region that would normally form a helical hairpin instead folds as a continuous helix (boxed). (C) View down the central receptor bundle.

Cubic-shaped crystals ($50 \times 50 \times 50\ \mu m^3$) were grown from a mixture of 520 μM Tm14s, 457 μM CheA Δ354, and 121 μM CheW after 1 month by vapor diffusion from a 2 μL drop (1:1 mixture of protein and reservoir: 500 μL reservoir of 0.2 M sodium acetate trihydrate, 0.1 M Tris (pH 8.5), 15% w/v polyethylene glycol 4000). Crystals with a similar shape and size as those derived from $Tm14_S$ (residues 107−191) were grown after 1 month. The new crystals (from $Tm14_S$ residues 107−192) consistently diffracted to 3.5 Å resolution. Crystals were soaked briefly in cryoprotectant that consisted of 85/15% (v/v) reservoir solution with glycerol prior to data collection in a N_2 cold stream. Diffraction data were collected at 100 K with synchrotron radiation at beamline A1 at the Cornell High Energy Synchrotron Source (CHESS). Selenomethionine was also incorporated into the $Tm14_S$ (residues 107−192) to aid in efforts to determine the helical registry, but unfortunately, the selenomethionine incorporated protein did not produce crystals.

Crystal Structure Determination and Refinement. Diffraction data were processed with HKL2000.[66] Initial phases were obtained with molecular replacement in PHASER[67] employing the 4.5 Å ternary complex structure with $Tm14_S$ (107−191) (PDB 3UR1) as a search model. The $Tm14_S$ subunits were manually unfolded and built into the resulting electron density with XFIT.[68] The resulting structure was refined with PHENIX.[69] B-factor sharpening[70] and composite omit-map calculation in PHENIX approved maps and allowed for proper interpretation of the $Tm14_S$ unzipping.

Bioinformatics Software and Data Sources. Sequences of CheA, CheW, and MCP proteins were retrieved from the MiST2 database[71] using sets of domain definitions that are specific for each protein, as described previously.[49] MCP sequences were classified using custom hidden Markov models.[28] Pairwise sequence alignments were built using BLAST v.2.2.17[72] with default parameters. Multiple sequence alignments were constructed in MAFFT v.6.0[73] with its L-INS-I algorithm. The conservation pattern was analyzed in Jalview[74] using underlying tools. Minimum evolution and maximum-likelihood phylogenetic trees of CheW protein sequences were constructed from the corresponding multiple sequence alignment and analyzed using the MEGA5 package.[75] Operons were predicted based on intergenic distances.[76] A protein cutoff scanning technique[77] with a β-carbon distance of 6 Å was used to prospect contact sites from PDB files of the cocrystal structures. Measurements were carried out using a custom Perl script, which compares the coordinates of every other β-carbon to the query atom in an all-against-all matrix analysis.

RESULTS

Crystal Lattice Engineering. In efforts to improve the diffraction resolution of the original ternary complex crystals (PDB code 3UR1), modifications were made to the termini of the shortened Tm14 receptor ($Tm14_S$). The 4.5 Å resolution structure indicated that these termini contacted each other on the symmetry axes of the crystal lattice and thereby allowed the receptor dimers to stack "end-to-end" with aligned helices (Figures 1 and 2). Several new constructs were generated with shifted termini to perturb this principal lattice contact (see Experimental Procedures). One of these (residues 107−192) produced crystals that consistently diffracted to ∼3.5 Å resolution (Table 1). Ultimately, a new 3.2 Å resolution structure (PDB code 4JPB) was determined from these crystals by molecular replacement (MR) with the previous 4.5 Å structure as a probe (Table 1). MR revealed that the general placement of the CheW, P5, and $Tm14_S$ units were quite similar in the two crystals. Indeed, refinement of the original model against the new data gave R_{factor}/R_{free} values of 0.228/0.267 to 3.2 Å resolution. However, examination of the higher resolution electron density (Figure S2 of the Supporting Information) revealed that the helix

dx.doi.org/10.1021/bi400383e | *Biochemistry* 2013, 52, 3852−3865

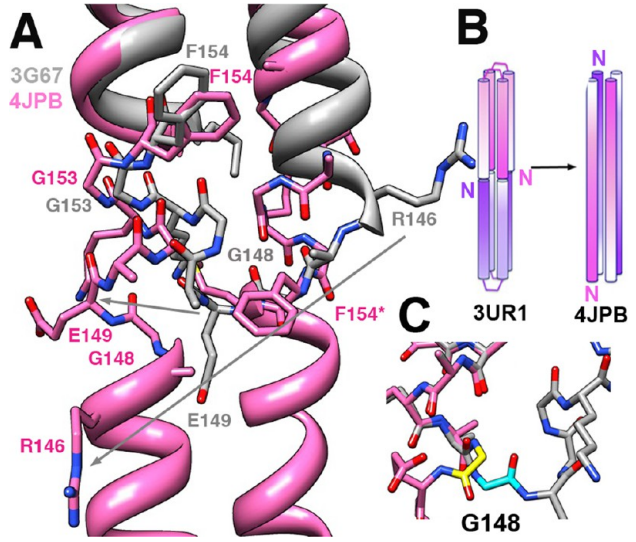

Figure 2. Unzipping of the $Tm14_S$ helical hairpin. (A) Superposition of one subunit of the Tm14 structure (3G67, gray) and two subunits of the unzipped $Tm14_S$ (4JPB, pink). Most of the residues in the transition region maintain similar backbone conformations in both structures, with the exception of Gly 148, whose ϕ/ψ angles change in 3G67 from values disallowed for Cβ-containing residues to α-helical (see (C)). Gray arrows map residues in the hairpin turn conformation to the extended conformation. The two $Tm14_S$ helices are antiparallel and offset from one another by two helical turns (note the position of Phe154 and its symmetry mate Phe154* in the opposing subunit). (B) Schematic depicting the relationship between two end-to-end hairpins in the previous ternary complex structure of 3UR1 and the tetrameric 4-helix bundle of 4JPB. Note helical hairpins of 3UR1 are inverted relative to that of superimposed 3G67 in (A). Color saturation of the helices decreases from N- to C-termini. (C) Superposition of Tm14 in 3G67 (gray) and in 4JPB (pink) over five residues N-terminal to Gly 148 shows how this residue switches from a Gly-specific conformation (cyan) to α-helical (yellow) in the tetramer.

register in the MR model was not compatible with the side-chain electron density. This was particularly true in the bundle core, where two invariant Phe154 residues appeared to be offset relative to their position in the structure of isolated Tm14 (PDB code 3G67). This consideration led to a new interpretation of the receptor structure, where the subunits had become "unzipped" and then associated into a tetramer of antiparallel helices (Figure 1). Refinement of the new configuration gave significantly improved refinement statistics (R_{factor}/R_{free} = 0.196/0.220; Table 1). Related fragments of $Tm14_S$ have been studied in complex with CheA and CheW by solution NMR, where they are primarily dimeric.[63,64] Indeed, $Tm14_S$ appeared largely dimeric on initial size-exclusion chromatography, but analysis of concentrations close to those used for crystallization by multiangle light scattering indicates a mixed species that exchanges between tetramers and dimers (Figure S1 of the Supporting Information). One possible explanation for the unzipping and tetrameric association may be linked to construct design. In addition to the native residues of the receptor, the expression construct introduced four non-native residues at the Tm14s N-terminus (Gly-Ser-His-Met-Ser_{107}-). Assuming that Ser107 holds the same position in the helical heptad repeat as it does in the structure of mostly complete Tm14 (PDB code 3G67), the non-native His would reside in a "d" position, internal to the hydrophobic core of the bundle. Two His side chains (one from each subunit) directed at each other in the bundle core would clash. Thus, their introduction may have destabilized the $Tm14_S$ hairpin dimer under the conditions of crystallization.

Molecular Arrangement within the Ternary Complex Crystal. Despite the switch from a dimeric to a tetrameric $Tm14_S$, the arrangement of components in this new structure (4JPB) and 3UR1 are quite similar. The conformational changes in the tip that allow for the unzipping of the helical hairpin and the switch from two end-end dimeric hairpins to an antiparallel tetramer of unzipped helices are centered in Gly148 and to lesser extent Gly151 (Figure 2). The Gly148 ϕ/ψ angles change from a region of Ramachandran space disallowed for β-carbon containing residues to the helical region; Gly151 changes conformation more slightly to allow for an i to i+4 main-chain hydrogen bond between Ala150 and Phe154. The Gly rearrangements in the extended tip (residues 147−153) produce a typical heptad repeat of 4-helix coiled-coils with Ala147 and Phe154 residing in the most buried "d" position (Figure 2). Adjacent antiparallel helices of the tetramer pack similarly as in Tm14 or other MCP structures (3G67, 2CH7, 1QU7, 3ZX6), but the symmetry-related helices from the other two subunits are shifted by approximately one helical turn relative to the first pair. This produces a ladder of the four internal Phe154 residues at the center of the bundle. Importantly, the structure presents a pair of antiparallel helices to CheW and P5 as would be found in a typically folded MCP receptor, but the two sides of the bundle (colored purple and pink in Figures 1−5) produce independent binding surfaces offset from one another.

The crystallographic asymmetric unit of 4JPB contains one subunit of CheW and one subunit of the CheA P5 domain, each interacting at a different position on the tetrameric receptor (Figure 1B), with P5 close to the center (lower position; Figure 1B) and CheW at the end (upper position; Figure 1B). Like in the low-resolution structure (3UR1), the *R*32 crystal symmetry generates rings of alternating CheW and P5 domains (Figure 1AC). Each ring contains three copies of CheW and three copies of P5 (Figure 1C). Each pair interacts through the ends of their β-sheets, with subdomain 1 of P5 binding subdomain 2 of CheW, as previously characterized in complexes of CheA with CheW.[34,52,62] However, to complete the ring, CheW subdomain 1 also interacts with P5 subdomain 2 in a contact pseudosymmetric to the first (Figure 3). Because CheW and P5 have similar folds, the rings have pseudo 6-fold symmetry. A receptor helix associates with the groove between the two β-barrels of each domain and thereby also produces a pseudo-6-fold symmetric arrangement of receptors. CryoEM in concert with the low resolution structure suggested that in native membrane arrays, one trimer-of-receptor-dimers associates at each P5 or CheW binding site.[24,62] Because of membrane incorporation of the native receptors, all of the tips would engage the CheW/P5 rings from the same direction, rather than with the alternating polarity found in both 4JPB and 3UR1 (Figure 1). In the unzipped receptor configuration of 4JPB, the $Tm14_S$ helix that primarily binds CheA-P5 does so in a region that would normally be N-terminal to the hairpin tip (this binding helix will henceforth be referred to as the "N-terminal helix"). CheW binds the very N-terminal end of this same helix, but does so with the binding groove flipped over relative to that of P5 (Figure 4). Thus, in the extended crystal lattice, two facing CheW/P5 rings are bound at their edges by six receptor tetramers that alternate their orientation around the rings from "up" to "down" (Figure 1). In 3UR1, weak electron densities for the CheA P4 domains were observed in large pockets below the rings at positions consistent with linkage to P5. In the new structure, the P4

dx.doi.org/10.1021/bi400383e | *Biochemistry* 2013, 52, 3852−3865

Table 1. Data Collection and Refinement Statistics for Ternary Complex Crystal Structure

wavelength (Å)	0.97700
spacegroup	*R*32
cell parameters	a = 213.99 b = 213.99 c = 208.19
resolution (Å)	46.2−3.2 (3.3−3.2)[a]
no. of observations	169251
no. of unique reflections	30554
redundancy	5.5 (3.9)[a]
completeness (%)	99.7 (99.2)[a]
R_{merge}[b]	0.105 (0.513)[a]
$I/\sigma(I)$	20.3 (1.4)[a]
Refinement statistics	
resolution range (Å)	46.2−3.2 (3.3−3.20)[a]
R factor, %	19.6 (33.6)[a]
R_{free}, %	22.0 (36.9)[a]
molecules/asym unit	1 P4−P5, 1 CheW, 2 $Tm14_S$ subunits (107−192)
residues/asym unit	576
solvent content (%)	84
overall *B*-value (Å^2)	36.1
main-chain *B*-value (Å^2)	32.9
side-chain *B*-value (Å^2)	39.5
Wilson B-value (Å^2)	40.5
Geometry	
bonds rmsd (Å)	0.01
angles rmsd (°)	1.33
Ramachandran plot, %	
most favored	89.6
additionally allowed	9.5
generouslly allowed	0.7
disallowed[c]	0.2

[a]Highest resolution range for compiling statistics. [b]$R_{merge} = \Sigma\Sigma_i |I_i - \langle I \rangle| / \Sigma\Sigma I_i$. [c]P5 residue 550 and CheW residue 87 are in disallowed ϕ/ψ regions but have well-defined electron density.

domains localize to the same general positions but appear even less well ordered with their electron densities falling off rapidly beyond the linkage to P5.

CheW Interaction with CheA-P5. In both 4JPB and 3UR1, P5 and CheW produce rings composed of 12 β-barrels, each β-barrel representing a subdomain from either P5 or CheW (Figure 2). At the interfaces formed between subdomains of opposing proteins, three antiparallel β-strands ($\beta3'$-$\beta4'$-$\beta5'$ for subdomain 1, and $\beta3$-$\beta4$-$\beta5$ for subdomain 2) wrap hydrophobic surfaces against each other in an antiparallel fashion (i.e., the $\beta3'$-$\beta4'$ loop of P5 subdomain 1 interacts with the $\beta4$-$\beta5$ loop of CheW subdomain 2 and $\beta3'$-$\beta4'$ loop of CheW subdomain 1 interacts with the $\beta4$-$\beta5$ loop of P5 subdomain 2; Figure 3). The higher resolution structure (4JPB) shows that Val, Leu, and Ile residues project similarly from $\beta3(')$-$\beta4(')$ on all four unique surfaces, but the loops connecting the strands differ considerably between the two proteins and also between the two subdomains (Figure 3). The sequence and structural variation within these loops likely gives rise to specificity for ring assembly. In agreement with experiment,[34,52,78] the interface between P5 subdomain 1 and CheW subdomain 2 is predicted to be stronger (880 Å^2 buried surface area per subunit; ΔG of formation = −13.6 kcal/mol; specificity P = 0.024[79]) compared to that between CheW subdomain 1 and P5 subdomain 2 (591 Å^2 buried surface area per subunit; ΔG of formation = −4.3 kcal/mol; specificity P = 0.282). The latter, "weaker" interaction has not been observed outside of the crystallized ternary complexes, although some mutational and modification data suggest that positions on this surface do have a functional role (vide infra).[55]

MCP Interactions with P5 and CheW. The higher resolution structure (4JPB) defines side chain contacts between the receptor helices and P5 or CheW. The junction between the two subdomains of either P5 or CheW harbor branched hydrophobic residues (kinase P5/CheW: kI560/wV27, kI563/wI30, kL547/wL14, kI566/wV33, kL629/wV98) that form a groove to bind the receptor N-terminal helix (Figure 4A,B). The receptor helix binds into this region on P5 with a row of exposed hydrophobic residues (rIle135, rLeu138, rIle142) as well as rAsn139, which provides two key hydrogen bonds to the peptide backbone of kIle566 on the extension of $\beta2$ that connects the subdomains (417 Å^2 buried surface area per subunit; ΔG of formation = −5.2 kcal/mol; P = 0.287). Mutagenesis studies in *E. coli* have strongly implicated Asn139 in chemoreceptor array structure and function,[80] and the hydrogen bonding interactions it makes likely serve as an anchor for P5 relative to the receptor tip (Figure 4A). Another potential anchoring contact involves the side-chain to main-chain hydrogen bonds between rArg146 and the kAsp564 at the periphery of the interface. Mutants of the corresponding Arg residue in Tsr (residue 388) were found to impair or abrogate chemotaxis responses in *E. coli*.[81]

The interface between CheW and $Tm14_S$ involves the analogous residues on CheW as on P5 (Figure 4B, see above), but the receptor contact forms from a stretch of hydrophobic side chains (rIle109, rLeu113, rIle116) three heptads N-terminal to the P5 contact (331 Å^2 buried surface area per subunit; ΔG of formation = −4.7 kcal/mol; P = 0.247). Moreover, Glu114, which follows the central hydrophobic residue also makes side-chain to main-chain hydrogen bonds with the extension of $\beta2'$, in

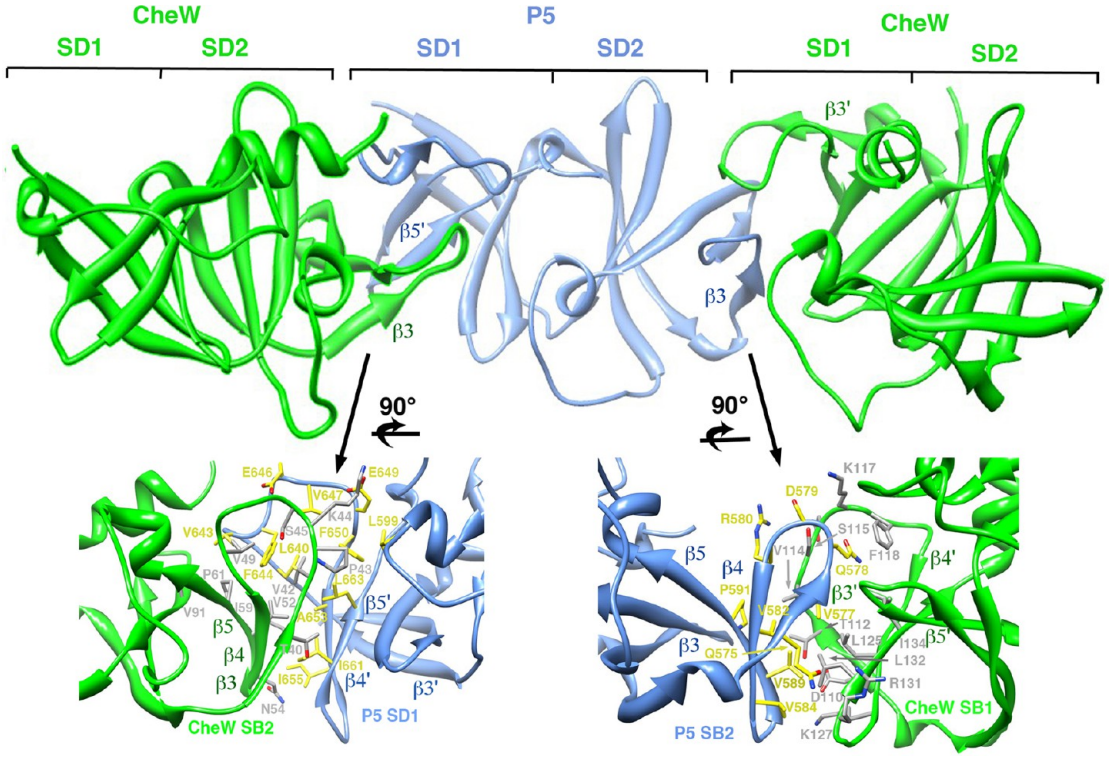

Figure 3. Pseudosymmetric contacts made by the CheW and P5 subdomains. (Top) Half of one P5-CheW ring viewed from the center. (Bottom) The interfaces formed between CheW-subdomain 2 (SB2) and P5-subdomain 1 (SB1) or P5-SB2 and CheW SB1 rotated 90° relative to their orientation above. The two contacts are very similar, with both involving close associations of the *β*3-*β*4-*β*5 to *β*3′-*β*4′-*β*5′ strands on the respective domains and the conserved hydrophobic residues conserved therein. Nonetheless, substantial differences in the *β*3(′)-*β*4(′) loops generate specific interactions.

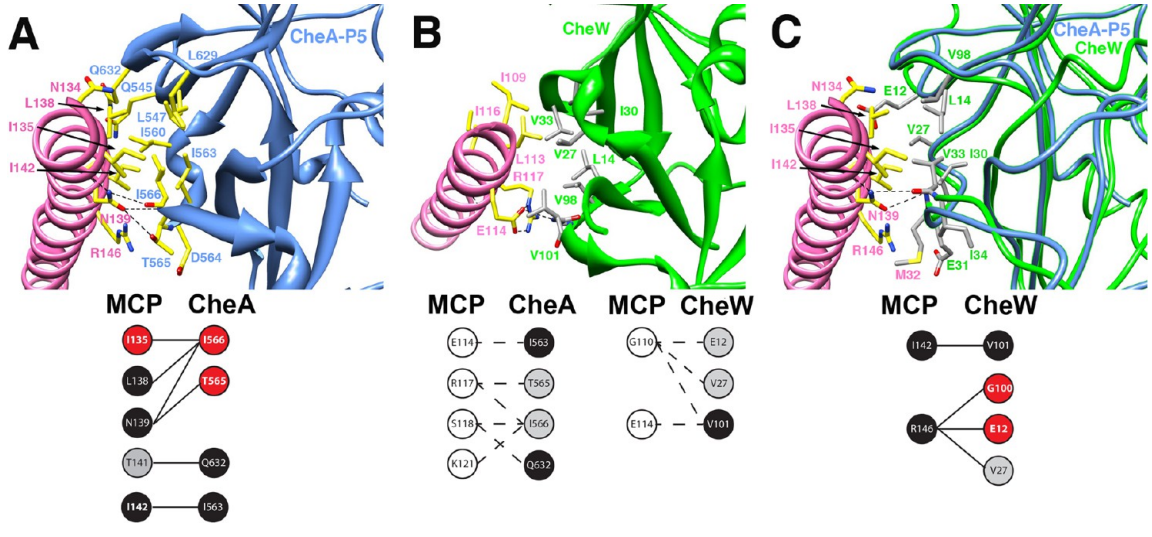

Figure 4. Interactions between $Tm14_S$ and P5 or CheW. (A) Contact between the N-terminal helix of $Tm14_S$ (magenta, N-terminus up) and the groove between subdomain 1 and 2 of CheA P5 (blue). Residues in the interface (yellow bonds) are primarily hydrophobic, with the exception of $Tm14_S$ rAsn139 which hydrogen bonds with the main-chain of P5 kIle566 on the connection between *β*2 and *β*3 and the kThr565 side chain. Below: Binding spots on MCP for CheA predicted by evolutionary information. White circles represent low sequence conservation in a given position (<80% consensus, no functional conservation); gray circles represent strong sequence conservation (>95% consensus, functional conservation); black circles represent the strongest sequence conservation (100% consensus, identical residues or the same charge conservation); red circles represent positions with correlated mutations. Solid lines identify contacts whose evolutionary history is consistent with the correlated mutation hypothesis; dashed lines identify contacts whose evolutionary history is inconsistent with the correlated mutation hypothesis. (B) Contact between the N-terminal helix of $Tm14_S$ and CheW. The $Tm14_S$ helix (pink) runs in the same direction as in (A), but CheW (green) is rotated ∼180° relative to P5. Because of the pseudosymmetry of the P5/CheW domains, the contact is very similar as in (A), with hydrophobic packing central to the interface and a side-chain-to-main-chain hydrogen bonds between rAsn114, and wVal98, which resides on the connection between *β*2′ and *β*3′. Below: Evolutionary analysis suggests that this receptor site does not constitute a conserved interaction for either CheW or CheA. (C) Superposition of CheW on to P5 demonstrates that CheW conserves chemical character of the residues (gray) at many of the key positions that mediate the contact between $Tm14_S$ and P5. Below: Evolutionary analysis supports this binding mode for CheW. Orientation same as in (A).

dx.doi.org/10.1021/bi400383e | *Biochemistry* 2013, 52, 3852−3865

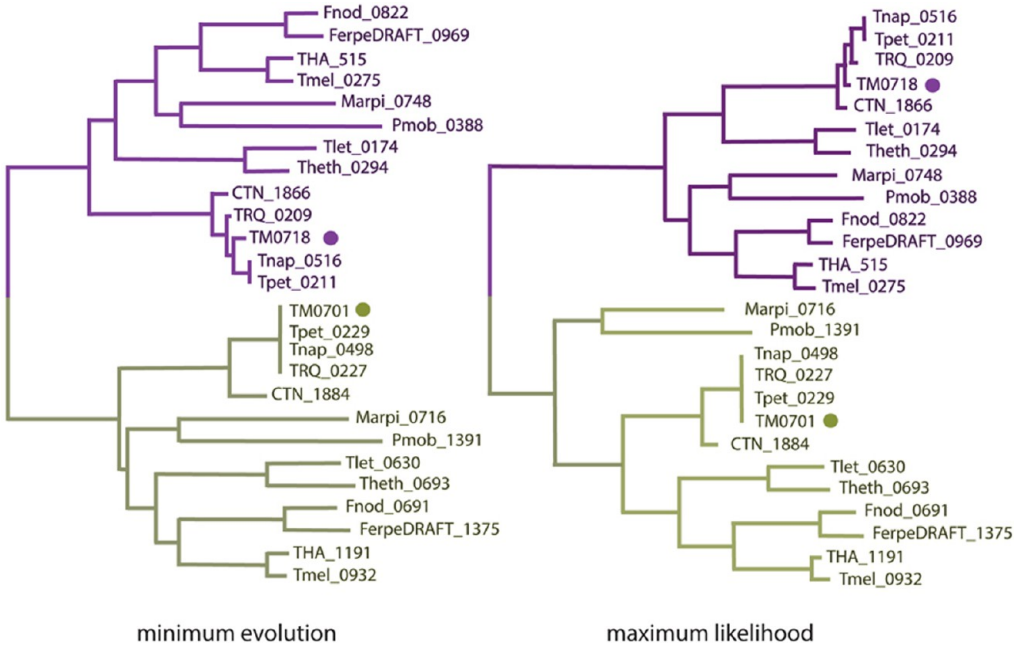

Figure 5. Minimum evolution and maximum likelihood phylogenetic trees showing two groups of CheW orthologs from Thermatogae. CheW1 group is shown in green and CheW2 group is shown in purple. Sequences are represented by their locus tag numbers. Sequences from *T. maritima* are labeled by circles.

close analogy to rAsn139 with β2 in the P5 contact. Thus, the upper CheW binding surface of $Tm14_S$ has a similar chemical character compared to the lower surface that engages P5, but the receptor helix runs across the binding groove in the opposite direction. Nonetheless, the intrinsic pseudo-2-fold symmetry of CheW that relates the subdomains essentially compensates for the reversed helix and produces an interaction analogous to that seen with P5 at the lower position.

The upper binding site of CheW, and hence the second P5/CheW ring, is not accounted for by the current models of array structure, which indicate all of the CheW:P5 units are found in one plane, at the tip of the receptors.[24,62] It is then likely that the upper CheW binding site facilitated crystal lattice formation by mimicking the actual site, which is located at the lower position (residues r135-r146). In support of this notion, rIle135, rIle136, rLeu138, and rIle142 and all undergo chemical shifts in solution NMR studies of CheW binding,[63] PDS measurements of spin-labeled proteins localize CheW to the lower site,[61] and genetic and biochemical experiments are consistent with this docking arrangement.[54,82−84] Indeed, superposition of CheW onto P5 indicates an excellent fit with the $Tm14_S$ 135−146 motif into the CheW groove (Figure 4C). However, the strong similarity between the upper and lower receptor binding motifs should not be completely dismissed and raises the possibility of multilayered rings mediated by such contacts in other contexts, perhaps involving receptor systems that are not membrane associated.

Computational Prediction of Protein Binding Sites. We sought to apply a computational genomic approach to independently predict CheW and P5 binding sites on MCP and project what relevance the interactions found in the ternary complex structure may hold in the context of the greater genomic landscape. Rapid accumulation of genomic data in recent years allows productive comparative sequence analyses to identify residues conserved through evolution that are important for structure and function, including protein−protein interactions. A "correlated mutation" hypothesis states that destabilizing changes in one position can be fixed by a compensatory modification nearby.[85] The relationship between correlated mutations can be derived from multiple alignments of protein sequences; however, due to the complexity of protein−protein interactions (e.g., mutually dependent residues may not necessarily be in direct contact), there is no single method or approach to successfully predict contact sites. In the case of the chemotaxis system, interacting proteins (MCPs, CheA and CheW) evolve in various subclasses with different protein interaction networks.[86] This essentially prohibits the application of statistical methods, such as "direct coupling analysis",[87] that rely on very large data sets of uniformly interacting proteins. To circumvent this problem and provide direct correlations to the available structural data, we conducted a comparative genomic analysis of the chemotaxis system of *T. maritima* within the well-defined limits of its specific subclass F1[86] and taxonomic position (phylum Thermotogae).

First, we retrieved sets of CheA, CheW, and MCP protein sequences from all available genomes of organisms from Thermotogae. A comprehensive list of these proteins can be found in Table S1 of the Supporting Information. Satisfactorily, all genomes of Thermotogae contained a single CheA protein that was confidently assigned to the F1 class.

Two Distinct CheW Proteins Are Present in Thermotogae Genomes. We have analyzed the sets of CheW and MCP sequences to reveal potential diversification within these protein families in Thermotogae. Phylogenetic trees constructed from a multiple sequence alignment of CheW protein sequences revealed two distinct sets of orthologs exemplified by *T. maritima* TM0701 (termed CheW1, and the protein contained in the structure presented herein) and TM0718 (termed CheW2): The longest branches on both minimum evolution and maximum likelihood trees separate the two classes (Figure 5). This classification is independently validated by the fact that all *cheW1* genes were found in operons together with *cheA* genes, whereas no *cheW2* genes were a part of these operons. Although this

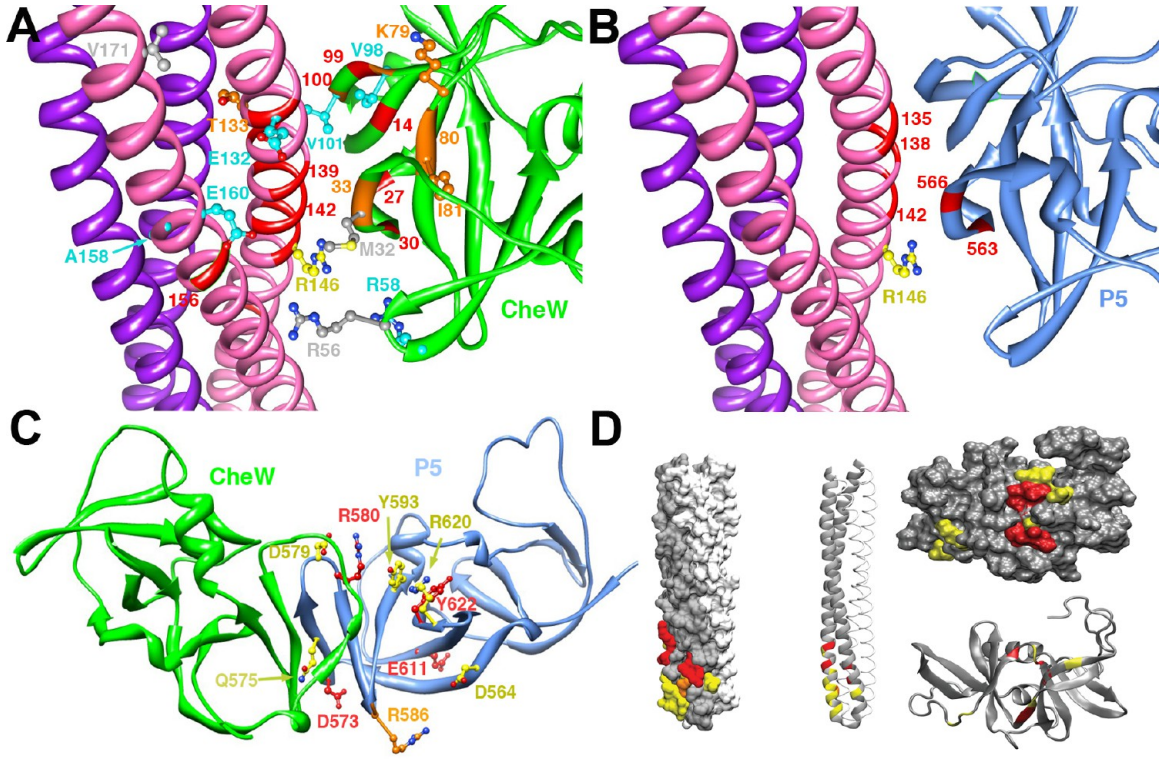

Figure 6. Structure–function analysis of ternary complex interfaces. (A) Residue positions known to report on or affect the interaction between CheW and receptors shown on the model of CheW bound to $Tm14_S$ based on superpositioning CheW onto P5 bound at the receptor tip (Figure 4C). Mutations of CheW residues known to suppress Tsr mutations in *E. coli* are shown as side chains (*T. maritima* numbering). Residue color associates allelic specific suppressors, i.e., mutations at CheW sites that rescue function of mutations at only similar colored sites in the receptor, while at the same time being themselves defective in a wt receptor background (r132 with w98; r133 with w79,w81; r158 with w98, w101; r160 with w57, w58, w101; r171 with w32,w56).[84] Orange (and red) ribbons represent CheW mutations or modifications defective in receptor interactions (w27, 30, 31, 32, 33, 35, 80, 81, 98, 101).[82−84,99] Residues identified as mediating $Tm14_S$-CheW contacts in solution NMR studies shown as red ribbons (w27, 98, 14, 30, 99; r132, 137, 139, 140, 141, 142, 143, 145, 146, 156).[63] R146 (yellow bonds) resides at the tip of the MCP hairpin and different residue substitutions at this site can produce locked "on" or "off" kinase behavior. (B) Residues found by solution NMR studies to mediate Tm14–P5 interactions are shown as red ribbons (k563, k566; r135, r138, r142).[64] (C) Sites of mutation or modification in P5 subdomain 2 that affect function. Residue positions depicted upon mutation or modification produce chemotaxis defects (red side chains; k573, k586, k580, k611, k622), curtail CheW binding (orange side chain r586 and rG587 - not shown) or prevent ligand from deactivating kinase (yellow side chains; k575, k579, k564, k593, k620).[54−56] (D) Correlation between bioinformatics and NMR data for predicting CheW interaction with MCP. Left, CheW binding sites on MCP (solvent accessible surface and ribbon representations). Right, MCP binding sites on CheW. Residues predicted by "bottom-up bioinformatics" are in red. Residues identified by NMR are in yellow. Overlapping residues are shown in orange.

protein has not yet been experimentally characterized, strong conservation of sequence and structure of the CheW2 protein suggests that this protein is functional in *T. maritima* and all its relatives.

Two Distinct MCP Classes Are Present in Thermotogae Genomes. All 117 MCP sequences from Thermotogae were matched against hidden Markov models (HMMs) constructed for specific MCP signaling classes.[28] Eighty sequences were confidently assigned to the 44H (44 helical heptads) class (Table S1 of the Supporting Information), which is the main MCP class within the F1 chemotaxis system.[86] Further sequence similarity analyses revealed a highly conserved group of 12 MCPs exemplified by the Tm14 protein from *T. maritima* (TM0014). Twenty-four MCPs did not match to any HMM, were sporadically distributed among Thermotogae genomes (indication of horizontal gene transfer) and remain unassigned. The TM0014-type sequences were all composed of a signaling domain of 36 helical heptads, contained no other domains, and showed a very high degree of similarity. On the other hand, in sequence composition they did not match the previously described 36H MCP signaling class;[28] therefore, we termed the new class T36H.

One CheW for Each Class of MCPs. We established that genomes of Thermotogae contain two different classes of CheW proteins (CheW1 and CheW2) along with MCPs that also belong to two different classes (T36H and 44H), whereas there was only one CheA protein per genome. On the basis of this finding, we hypothesize that each of the two CheW proteins associates MCPs from each of the two classes with the same CheA protein. If so, which CheW is specific for which MCP class? The structure presented herein, coupled with other substantial experimental evidence, suggests that CheW1 (TM0701) interacts with the T36H MCP (TM0014).[62,63] Therefore, if our hypothesis is correct, then 44H MCPs should interact with CheW2. There is no experimental evidence to support this claim, because the CheW2 protein from *T. maritima* has been recalcitrant to recombinant production (data not shown). However, we can offer the following computational evidence in support of this hypothesis. It is a well-established fact in evolutionary molecular biology that if two proteins interact they coevolve.[85] Indeed, CheW1 and T36H proteins appear to be confined to the phylum Thermotogae, whereas CheW2 and 44H proteins are widely distributed throughout the prokaryotes.[86] For example, the sequence similarity score between CheW1 from

T. maritima and CheW protein from *E. coli* is only 42.4 bits (26% identity), whereas that between CheW2 and the *E. coli* protein is 97.4 bits (37% identity) (Figure S3 of the Supporting Information).

If CheW1 interacts with T36H MCPs and CheW2 interacts with 44H MCPs, then class-specific residues in both protein families (CheW1 versus CheW2 and T36H versus 44H) are candidates for the given interaction. Analysis of the multiple sequence alignments constructed from CheW1 and CheW2 sequences (Figure S4 of the Supporting Information) and T36H and 44H MCPs (Figure S5 of the Supporting Information) revealed several positions in both sets of proteins, where correlated mutations have occurred. For example, a position corresponding to Glu12 in CheW1 (TM0701) is 100% conserved as a negative charge in CheW1 orthologs (in one sequence Glu is changed for Asp); however, the same position in CheW2 orthologs is a positive charge (Lys, 100% conserved). Similarly, the only position, where a reciprocal change is seen in the MCP set is Arg131 in TM0014, which is invariably conserved in all T36H MCPs, whereas all 44H MCPs have a negative charge (Glu, 100% conserved). Thus, according to the correlation mutation hypothesis, corresponding positions in CheW and MCP are mutually dependent; e.g., they may interact. The direct interaction between these two residues is not seen in the ternary complex structure because CheW binds at the upper site in the lattice, most likely due to competition between CheW and P5 for the actual lower binding site. The superposition of CheW onto P5 (Figure 4C) predicts that both residues should reside at the edge of the CheW MCP interface, but will not contact each other. Nonetheless, in functioning arrays CheW and MCPs could sample a range of related association modes, some of which may bring these residues into closer contact. Furthermore, the rArg131−wGlu12 interaction may participate in the recognition of specific receptors by specific adaptors (vide infra). Satisfactorily, this finding is further supported by recent NMR studies, where some of the residues showing significant chemical shift changes upon MCP-CheW binding were identified in very close proximity: rGlu132 (next to rArg131) in $Tm14_S$ and wLeu14 (next to wGlu12) in CheW1.[63] Other positions with correlated mutations in CheW (wAsp28, wLys36, wAsp38, wGly100, wLys121) and MCP (rThr141, rAsn159, and rGlu162) are also located in the vicinity of residues that showed significant chemical shift changes upon MCP-CheW binding (Figure 6). Most importantly and in summation, all predicted CheW-binding sites are located at the MCP tip, in agreement with the 3UR1 structure.

"Top-Down" Comparative Genomic Analysis. "Bottom-up" correlated mutation analysis that predicted CheW−MCP interaction sites cannot be used for predicting CheA−MCP interaction sites, because there was only one set of orthologous CheA proteins available for Thermotogae. However, we employed a "top-down" approach, where the evolutionary histories of the interaction sites prospected from the crystal structure were analyzed for consistency with the correlated mutation hypothesis. For example, if a pair of residues in two proteins is predicted to be an interaction site, they should both be well conserved (e.g., invariable, charge preservation, etc) or show a correlated mutation pattern. This approach can be equally applied to MCP−CheA and MCP−CheW interactions, which enabled us to analyze all four putative binding interfaces revealed in two cocrystal structures (Tables S2−S4 of the Supporting Information). Contact sites in interacting proteins were assigned using a protein cutoff scanning technique[77] and are shown in Table S2 of the Supporting Information. We then used multiple sequence alignments to trace the evolutionary history of each residue in proposed contacts and analyzed it for consistency with the correlated mutation hypothesis (Tables S3−S5 of the Supporting Information), which states that if contact between two residues is evolutionarily conserved, they will either be invariant or change together in a correlated manner. Summarized results are shown in Figure 4 in reference to the predicted interfaces. Strikingly, in Thermotogae the evolutionary histories of all six MCP−CheA contact pairs and all four MCP−CheW pairs prospected from the top binding site of the MCP are inconsistent with the correlated mutation hypothesis. In a similarly striking contrast, all six MCP−CheA contact pairs and all four MCP−CheW pairs identified at the tip of MCP have evolutionary histories fully consistent with the correlated mutation hypothesis. Furthermore, in both MCP−CheW and MCP−CheA interactions at the tip, there were true correlated mutations. While Arg146 in all MCPs remains fully conserved, its interacting residues in CheW show a correlated mutation pattern. Glu12 and Gly100 are mutually dependent (Figure S4 of the Supporting Information): Glu12 in CheW1 becomes Lys in CheW2, and Gly100 in CheW1 becomes Glu in CheW2. These residues are mutually dependent, most likely because they both interact with the invariable positive charge (residue 146) in MCPs. The pattern of covariance in MCP−CheA interaction is different, but similarly convincing: rIle135 in Tm14 is mutually dependent with kIle566 and kThr565 in CheA. Indeed, rIle135 directly contacts kIle566 in the crystal structure (Figure 4).

Taken together, the evolutionary history of contact sites assigned from the complex crystal structures strongly suggests that (i) both CheW and the P5 domain of CheA bind to the tip of MCP and (ii) MCP contact sites for CheW and CheA binding are not identical, although there is a substantial overlap.

DISCUSSION

The 3.2 Å resolution structure of the *T. maritima* ternary complex differs from the 4.5 Å resolution 3UR1 structure primarily in the modeling of the $Tm14_S$ receptor. First, the 3UR1 structure contains four end-to-end hairpin dimers instead of a tetramer of continuous helices. Second, the location of the CheW/P5 binding surface on the receptor is shifted roughly one turn of helix relative to the current structure. In the higher resolution structure, clear side-chain electron density makes $Tm14_S$ placement certain, whereas in the lower resolution structure, side chains were not discernible, and thus the receptor fragment was placed based on the apparent positions of the termini.[62] Finally, the polarity of the helical bundles are switched between the structures, which effectively changes the engagement of the lower binding motif from CheW to CheA P5. These considerations raise the question as to whether the lower resolution data would be better modeled by the new structure derived from the higher-resolution data. Difference Fourier maps calculated between the experimental amplitudes from the two data sets show large peaks at the junctions where the hairpins have unzipped, which suggests the structures may be different in this region (Figure S2B of the Supporting Information). Agreement statistics derived from refinement of the old and new models against the low resolution data slightly favor the new receptor configuration, but do not greatly distinguish between the two models (R_{factor}/R_{free}(old) = 0.207/0.238; R_{factor}/R_{free}(new) = 0.206/0.217). Biochemical analysis of intact arrays, similar to those performed in the companion paper on CheA P5 are needed to verify the detailed CheW $Tm14_s$ interface defined

in 3UR1. Despite this uncertainty, given the arguments presented herein, it is likely that the interactions of receptor with CheW are very similar to those of receptor with CheA-P5. Thus, the overall arrangement of receptors, CheA and CheW in the current array models[24,62] continues to be supported by nearly all available data.

There is a growing consensus over the structure of membrane associated bacterial chemotaxis receptor arrays, which appear to be universally based on a hexameric assembly of receptors that form trimers-of-receptor dimers, with the greatest ordering at their membrane distal tips where CheA and CheW bind.[14,22,25,62,88] Recent electron cryotomographic data combined with the modeling of crystallographic structures suggest that CheA and CheW form ring structures of pseudohexagonal symmetry that template the receptors, for at least some states of the arrays.[24,62] Interdigitated assembly states of overexpressed chemoreceptors, where antiparallel dimers associate through their tips have also been described, but are unlikely to be functional.[21] The "unzipped" tetrameric assembly for an MCP subunit described here has not been previously observed, and may well result from the shortened $Tm14_S$ fragment that contains several N-terminal non-native residues at its termini. A similar $Tm14_S$ fragment has been used in NMR studies, where the subunits form helical hairpins and behave as typical MCP dimers.[63,64] Nonetheless, it is worth noting that full-length Tm14 is a naturally "soluble" receptor, in that it has no transmembrane region.[35] Computational genomics indicates that CheW1 is specific for this class of receptor (T36H). Soluble MCPs have been observed in other settings, where they have important functions.[89−92] In some cases these receptors localize to the receptor arrays, whereas in others, they appear to form cytoplasmic clusters.[89−92] Given the relatively modest conformational changes in the tip that allow for the switch between dimeric and tetrameric states, the possibility that some classes of soluble receptors form extended unzipped structures should not be ruled out. Certainly, substantial rearrangements of coiled-coils play important roles in other systems. Most notably, membrane fusion events involve large-scale conformational changes and repacking of helical proteins. These processes include SNARE mediated vesicle fusion[93,94] and viral envelope fusion.[95] In the latter case, viral fusion proteins have hairpin-like helical structures morph into long extended coiled-coil trimers to associate the viral envelope with the plasma membrane.[95−98] Thus, if soluble MCPs were to unzip and repack, these other processes demonstrate that such changes would not meet a prohibitive thermodynamic barrier.

Despite the unusual tetrameric assembly of $Tm14_S$, the interfaces found among CheA, CheW, and MCPs in this ternary complex structure are representative of those found in the transmembrane chemosensory arrays. Sequence conservation, as well as the coevolution of interacting sites, strongly supports the groove between subdomain 1 and 2 on both P5 and CheW as being the primary binding location for CheA and CheW on MCPs. For the receptor, the evolutionary analysis only supports the lower, tip-proximal binding site as being the recognition motif for both CheW and P5. Although the current high-resolution structure does not have CheW bound at this position, superposition of CheW with P5 generates an interface that was predicted by computational genomics (Figure 4), is consistent with the hexagonal symmetry of the native receptor arrays, and was anticipated by a large body of additional experimental data. NMR chemical shift perturbations implicate residues on both CheW and $Tm14_S$ that are found within this contact[63,64] (Figure 6A,D). Pulsed dipolar ESR experiments of spin-labeled ternary complexes of $Tm14_S$, CheA and CheW combined with targeted disulfide cross-linking also place CheW at the tip of the receptor in close proximity of the lower binding site.[61] In addition, allele-specific mutations of CheW that suppress defective Tsr receptors with mutations near or in the lower binding site map to the CheW binding groove[84] (Figure 6A). Allele-specific suppressor mutations on two genes can imply that the derived proteins interact with one another. Nonetheless, other coupling mechanisms are also possible. Hence, it is quite remarkable how closely sets of allelic specific Tsr/CheW suppressor mutations localize to the predicted interface between $Tm14_S$ and CheW (Figure 6A). Although mutational studies[82−84] and chemical modification/protection[54,99] also support the subdomain 1−2 groove on CheW as being the primary MCP binding site (Figure 6A), the suppressor studies genetically link this recognition motif directly to the corresponding surface on the MCP tip.[84] It should also be noted that there is one set of CheW/Tsr allelic suppressors that map closest to one another when only the upper binding site on $Tm14_S$ is considered (Figure S7 of the Supporting Information). Although it is tempting to interpret this data as evidence for functional relevance of the upper binding site, it is more likely that longer-range structural coupling through the receptor propagates the effects of this mutation to CheW binding at the lower position.

Several lines of evidence suggest that the lower binding site on $Tm14_S$ of the current structure represents the primary association mode of CheA with receptors. Specific residues on the receptor tip, where substitutions greatly perturb chemotaxis in *E. coli*, play critical roles in the interface with P5 at the lower site. For example, rAsn139 makes key hydrophilic contacts with partner proteins by hydrogen bonding directly with the main chain of kIle566 and wVal33 (Figure 4). Substitutions of the analogous residue in Tsr (Asn381) have dramatic functional effects, with all but a Gly substitution destroying chemotaxis.[80] In the context of the hexagonal arrays, Asn381 is also predicted to mediate receptor trimerization.[80] Thus, the near essential nature of this residue results from its participation in three distinct interfaces: those with CheA, CheW and two other receptor subunits. In another case, rArg146, which resides at the base of the lower interface (and at the boundary of the tip; Figure 4), hydrogen bonds with the main-chain of the connection to subdomain 2 and is close to forming a salt-bridge with kAsp564 (wGlu31). Substitutions to large residues at this site in Tsr (Arg388) produce either "lock-on" (Trp, Tyr) or "lock-off" (Phe, His) kinase activity.[81] Because of its potential to also mediate receptor trimer contacts on the adjacent subunit, these phenotypes also likely result from combined effects at multiple interfaces. Nonetheless, the mutational studies do suggest that alterations in structure at the interfaces resolved by the current structure could be critical for controlling kinase activity.

Despite considerable genetic and biochemical studies of CheA, there has been less direct functional data implicating the P5 surface that binds $Tm14_S$ in function.[54−56] This is probably because mutations or modifications at many sites affect P5 structure and CheW binding, and these properties are coupled to receptor interactions.[54−56] Nonetheless, NMR studies that rely on methyl-TROSY experiments of Thermotoga proteins identified the same interface defined by the structure and predicted by computational genomics (Figure 6B,D). Most importantly, the companion paper to this report[65] has taken a targeted disulfide cross-linking and mutagenesis (TAM-IDS) approach to define the CheA−receptor contacts in both isolated

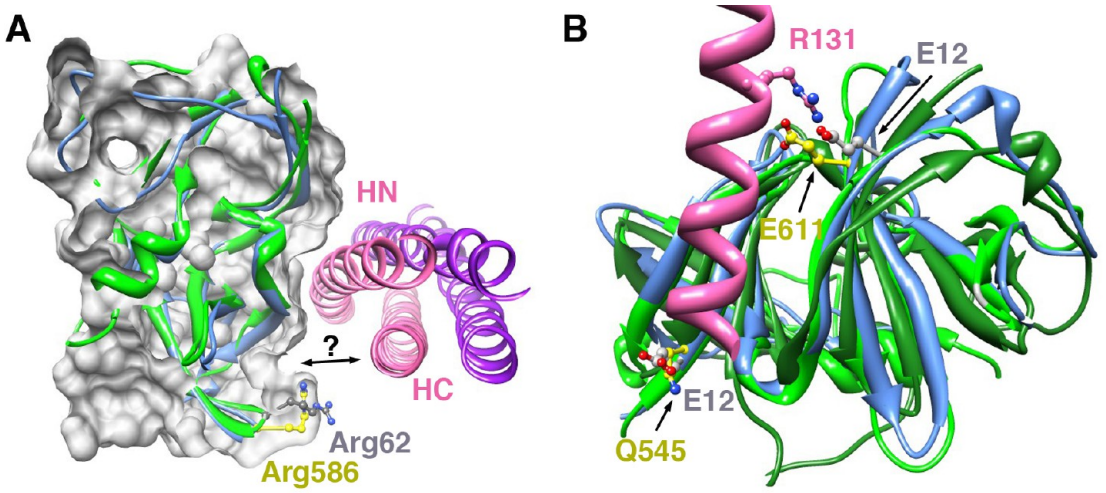

Figure 7. Hypothetical alternate interfaces in chemosensory clusters. (A) wArg62 (kArg586) is a mutational hotspot on CheW, but does not directly engage the receptor, which binds mainly through the N-terminal helix (pink, HN). A relative rotation of CheW (green ribbons, gray side chain), P5 (blue ribbons, yellow side chain) or receptor could engage subdomain 2 with the C-terminal helix (HC) in some states of the ternary complex. (B) wGlu12 (kQ545) and rArg131 show correlated changes in residue identity. If CheW subdomain 1 is superimposed with P5 subdomain 1 (CheW - light green ribbons, gray side chains, P5 - blue ribbons, yellow side chains) to maintain a similar directionality of helix binding, wGlu12 and rArg131 (pink) both participate in the interface, but do not contact. However, if subdomain 1 of CheW is superimposed with P5 subdomain 2 (CheW - dark green ribbons, gray side chains), wGlu12 corresponds to kGlu611 (yellow side chain) and would be positioned to salt-bridge with rArg131.

and cellular chemosensory arrays. These methods were able to distinguish the current interface from the one modeled on the 4.5 Å resolution structure and verify with considerable detail that the interface defined by the higher resolution structure functions in native arrays. Thus, P5 binds at the lower site on receptor tip in a similar orientation to CheW, and this at least partially explains the competition of CheA and CheW for overlapping sites on receptors.[59,100] The companion paper also shows that the receptor-P5 interaction plays an important role in receptor-mediated regulation of kinase activity.

Both ternary complex crystal structures contain large rings formed by the P5 and CheW subdomains that have been presumed to template receptor trimers in hexagonal arrays.[24,62] The ring contact between P5 subdomain 1 and CheW subdomain 2 contact has been characterized by a variety of approaches.[34,52,54−56,99] The secondary contact that completes the ring structures (subdomain 1 of CheW to subdomain 2 of CheA) has not been previously observed outside of crystal structures; however, mutational data and chemical modification experiments have implicated residues near this interface in function (Figure 6C). There are numerous sites in P5 subdomain 2 that when modified produce chemotaxis defects or affect CheW binding; however, many other modifications in subdomain 1 produce similar outcomes.[55,56] Notably, some Cys-substitutions (and subsequent modification) in subdomain 2 generate phenotypes in which CheA does not deactivate properly with chemoattractant.[55] Such behavior results only from subdomain 2 substitutions, and several reactive sites localize directly to the interface between subdomain 2 and CheW subdomain 1 (Figure 6C). Thus, modulation of this ring contact may play an important role in kinase regulation.

Despite our advancing understanding of the overall architecture and interactions within chemosensory arrays, there are many details to be resolved. Array function must involve transitions among different structural states that produce different levels of kinase activity. Recent computational work suggests that hexagonal lattice models may correlate with the active state of CheA, although this remains to be verified.[101]

Given what we know about the assembly modes and the large amount of biochemical and genetic data available on the chemotaxis system, can we infer additional interactions not visualized in the current structures? Although caution must be taken in the interpretation of mutational data due to the networked, potentially redundant nature of molecular interactions within the arrays, a few observations deserve note. For example, substitutions or modifications of wArg62 (*E. coli* CheW Arg56) dramatically affect MCP binding and chemotaxis;[83] however, this residue does not directly contact the receptor bundle, despite being oriented toward the C-terminal helix (Figures 4 and 7). Furthermore, mutations of Tsr that suppress CheW mutations at Arg62 and at other residues on the same β4-β5 loop that contains Arg62 map to exposed positions on the C-terminal helix of $Tm14_S$[84] (Figure 6A). Notably, Arg62 is also conserved as an Arg on P5 subdomain 2 (kArg586). Thus, in some states of the array, a relative rotation or deformation of the components may engage the end of subdomain 2 from CheW and/or P5 with the C-terminal helix of the receptor (Figure 7A). Indeed, the companion paper provides the first evidence that such a rotation occurs as targeted disulfide cross-links between kT565 (*S. typhimurium* E550C) and rI156 (Tsr V398C) form more rapidly in the presence of chemoattractant.[65] This change in reactivity is consistent with a closer association of P5 subdomain 2 and the receptor C-terminal helix when ligand inhibits CheA.

The correlated residue changes at w12 and r131 identified by bioinformatics in the two *T. maritima* CheW/receptor classes also reveal an intriguing structural relationship. The equivalent residue to wGlu12 in P5 does not contain a carboxylate (kGln545), but the pseudo symmetric residue on subdomain 2 does (kGlu611). kGlu611 makes a direct salt bridge with Arg131, which is the position that undergoes a correlated switch to Glu when w12 changes to Lys. Thus, if the lower binding site were to engage CheW with the N-terminal helix running in the opposite direction, w12 and r131 would salt bridge (Figure 7B). Note that this is the orientation that the N-terminal helix takes with respect to CheW at the upper nonconserved site (Figure 4B). At least for

CheW and Tm14 in solution, PDS and targeted disulfide cross-linking favor the CheW orientation that mimics that of P5.[61] Nonetheless, it may be possible in some instances for the CheW/P5 binding groove to accept a receptor helix with either polarity. An inverted arrangement that satisfies the w12-r131 pair would not be compatible with a membrane-associated array, where the receptors all project toward CheA/CheW from the same direction, but such constraints are not present for naturally soluble receptors clusters. Thus, the symmetry of their architectures could be different than those of the membrane arrays and may involve elaborations of the interfaces found in the current structures.

■ ASSOCIATED CONTENT

Supporting Information

Multiangle light scattering analysis of Tm14s; electron density maps of ternary structure; pairwise sequence alignments among CheW proteins from various species; sequence alignments of Thermotogae CheW proteins; sequence alignments of Thermotogae MCPs; sequence alignments of CheA P5 domains; allele specific repressor mutations between Tsr and CheW mapped onto the upper MCP interaction site; contact sites among components of the ternary structure; MCP contacts to CheW and CheA determined by various means. This material is available free of charge via the Internet at http://pubs.acs.org.

Accession Codes

Deposited in the Protein Data Bank under accession code 4JPB.

■ AUTHOR INFORMATION

Corresponding Author

*(B.R.C): E-mail: bc69@cornell.edu, Tel 607-254-8634; (I.B.Z) E-mail: joulineib@ornl.gov, Tel 865-201-1860.

Funding

Support provided by NIH Grants GM-040731 (J.J.F.), GM-072285 (I.B.Z.), and GM-066775 (B.R.C.)

Notes

The authors declare no competing financial interest.

■ ACKNOWLEDGMENTS

We thank the Cornell High Energy Synchrotron Source (CHESS) for access to data collection facilities. We also thank J. S. Parkinson (University of Utah) and F. W. Dahlquist (University of California, Santa Barbara) for helpful discussions regarding the placement of the receptor interaction region relative to CheA/CheW and K. Piasta (University of Colorado, Boulder) for general discussion and for sharing their data prior to publication.

■ ABBREVIATIONS USED

cryo-electron microscopy, cryoEM; FPLC, fast protein liquid chromatography; MCP, methyl-accepting chemotaxis protein; MCP_C, MCP cytoplasmic region; KCM, kinase control module; MR, molecular replacement; PDS, ESR, electron-spin resonance spectroscopy; P5, CheA regulator domain; PIR, protein interaction region; r, receptor; k, kinase; w, CheW; Tm14, *T. maritima* MCP TM0014; Tm14 PIR, $Tm14_S$; TAM-IDS, tryptophan and alanine mutation to identify docking sites; Tris, 2-amino-2-hydroxymethyl-propane-1,3-diol

■ REFERENCES

(1) Adler, J. (1975) Chemotaxis in bacteria. *Annu. Rev. Biochem. 44*, 341−356.

(2) Sourjik, V., and Wingreen, N. S. (2012) Responding to chemical gradients: bacterial chemotaxis. *Curr. Opin. Cell Biol. 24*, 262−268.

(3) Hazelbauer, G. L., Falke, J. J., and Parkinson, J. S. (2008) Bacterial chemoreceptors: high-performance signaling in networked arrays. *Trends Biochem. Sci. 33*, 9−19.

(4) Wadhams, G. H., and Armitage, J. P. (2004) Making sense of it all: bacterial chemotaxis. *Nat. Rev. Mol. Cell Biol. 5*, 1024−1037.

(5) Howitt, M. R., Lee, J. Y., Lertsethtakarn, P., Vogelmann, R., Joubert, L. M., Ottemann, K. M., and Amieva, M. R. (2011) ChePep Controls Helicobacter pylori Infection of the Gastric Glands and Chemotaxis in the Epsilonproteobacteria. *MBio 2*, No. 00098-11.

(6) Rader, B. A., Wreden, C., Hicks, K. G., Sweeney, E. G., Ottemann, K. M., and Guillemin, K. (2011) Helicobacter pylori perceives the quorum-sensing molecule Al-2 as a chemorepellent via the chemoreceptor TIpB. *Microbiology-Sgm 157*, 2445−2455.

(7) Rolig, A. S., Carter, J. E., and Ottemann, K. M. (2011) Bacterial chemotaxis modulates host cell apoptosis to establish a T-helper cell, type 17 (Th17)-dominant immune response in Helicobacter pylori infection. *Proc. Natl. Acad. Sci. U. S. A. 108*, 19749−19754.

(8) Schweinitzer, T., and Josenhans, C. (2010) Bacterial energy taxis: a global strategy? *Arch. Microbiol. 192*, 507−520.

(9) Antunez-Lamas, M., Cabrera-Ordonez, E., Lopez-Solanilla, E., Raposo, R., Trelles-Salazar, O., Rodriguez-Moreno, A., and Rodriguez-Palenzuela, P. (2009) Role of motility and chemotaxis in the pathogenesis of Dickeya dadantii 3937 (ex Erwinia chrysanthemi 3937). *Microbiology-Sgm 155*, 434−442.

(10) Spagnuolo, A. M., DiRita, V., and Kirschner, D. (2011) A model for Vibrio cholerae colonization of the human intestine. *J. Theor. Biol. 289*, 247−258.

(11) Li, C. H., Bakker, R. G., Motaleb, M. A., Sartakova, M. L., Cabello, F. C., and Charon, N. W. (2002) Asymmetrical flagellar rotation in Borrelia burgdorferi nonchemotactic mutants. *Proc. Natl. Acad. Sci. U. S. A. 99*, 6169−6174.

(12) Lux, R., Miller, J. N., Park, N. H., and Shi, W. Y. (2001) Motility and chemotaxis in tissue penetration of oral epithelial cell layers by Treponema denticola. *Infect. Immun. 69*, 6276−6283.

(13) Motaleb, M. A., Miller, M. R., Bakker, R. G., Li, C. H., and Charon, N. W. (2007) Isolation and characterization of chemotaxis mutants of the lyme disease spirochete Borrelia burgdorferi using allelic exchange mutagenesis, flow cytometry, and cell tracking, in *Methods in Enzymology* (Simon, M. I., Crane, B. R., and Crane, A., Eds.) Vol 422: Two-Component Signaling Systems, Part A, Academic Press, New York

(14) Maddock, J. R., and Shapiro, L. (1993) Polar location of the chemoreceptor complex in the *Escherichia coli* cell. *Science 259*, 1717−1723.

(15) Greenfield, D., McEvoy, A. L., Shroff, H., Crooks, G. E., Wingreen, N. S., Betzig, E., and Liphardt, J. (2009) Self-Organization of the *Escherichia coli* Chemotaxis Network Imaged with Super-Resolution Light Microscopy. *PLoS Biol. 7*, No. e1000137.

(16) Kim, C., Jackson, M., Lux, R., and Khan, S. (2001) Determinants of chemotactic signal amplification in *Escherichia coli*. *J. Mol. Biol. 307*, 119−135.

(17) Kim, S. H., Wang, W. R., and Kim, K. K. (2002) Dynamic and clustering model of bacterial chemotaxis receptors: Structural basis for signaling and high sensitivity. *Proc. Natl. Acad. Sci. U. S. A. 99*, 11611−11615.

(18) Goldman, J. P., Levin, M. D., and Bray, D. (2009) Signal amplification in a lattice of coupled protein kinases. *Mol. Biosyst. 5*, 1853−1859.

(19) Briegel, A., Ding, H. J., Li, Z., Werner, J., Gitai, Z., Dias, D. P., Jensen, R. B., and Jensen, G. J. (2008) Location and architecture of the Caulobacter crescentus chemoreceptor array. *Mol. Microbiol. 69*, 30−41.

(20) Khursigara, C. M., Wu, X. W., and Subramaniam, S. (2008) Chemoreceptors in *Caulobacter crescentus*: Trimers of receptor dimers in a partially ordered hexagonally packed array. *J. Bacteriol. 190*, 6805−6810.

(21) Zhang, P. J., Khursigara, C. M., Hartnell, L. M., and Subramaniam, S. (2007) Direct visualization of Escherichia coli chemotaxis receptor

arrays using cryo-electron microscopy. *Proc. Natl. Acad. Sci. U. S. A. 104*, 3777−3781.
(22) Khursigara, C. M., Lan, G., Neumann, S., Wu, X., Ravindran, S., Borgnia, M. J., Sourjik, V., Milne, J., Tu, Y., and Subramaniam, S. (2011) Lateral density of receptor arrays in the membrane plane influences sensitivity of the *E. coli* chemotaxis response. *EMBO J. 30*, 1719−1729.
(23) Briegel, A., Beeby, M., Thanbichler, M., and Jensen, G. J. (2011) Activated chemoreceptor arrays remain intact and hexagonally packed. *Mol. Microbiol. 82*, 748−757.
(24) Liu, J., Hu, B., Morado, D. R., Jani, S., Manson, M. D., and Margolin, W. (2012) Molecular architecture of chemoreceptor arrays revealed by cryoelectron tomography of *Escherichia coli* minicells. *Proc. Natl. Acad. Sci. U. S. A. 109*, E1481−E1488.
(25) Briegel, A., Ortega, D. R., Tocheva, E. I., Wuichet, K., Zhuo, L., Chen, S., Muller, A., Iancu, C. V., Murphy, G., Dobro, M. J., Zhulin, I. B., and Jensen, G. J. (2009) Universal architecture of bacterial chemoreceptor arrays. *Proc. Natl. Acad. Sci. U. S. A. 106*, 17181−17186.
(26) Falke, J. J., and Hazelbauer, G. L. (2001) Transmembrane signaling in bacterial chemoreceptors. *Trends Biochem. Sci. 26*, 257−265.
(27) Zhulin, I. B. (2001) The superfamily of chemotaxis transducers: From physiology to genomics and back. *Adv. Microb. Physiol. 45*, 157−198.
(28) Alexander, R. P., and Zhulin, I. B. (2007) Evolutionary genomics reveals conserved structural determinants of signaling and adaptation in microbial chemoreceptors. *Proc. Natl. Acad. Sci. U. S. A. 104*, 2885−2890.
(29) Parkinson, J. S. (2010) Signaling Mechanisms of HAMP Domains in Chemoreceptors and Sensor Kinases, in *Annual Review of Microbiology* (Gottesman, S., and Harwood, C. S., Eds.), Vol 64, pp 101−122.
(30) Hulko, M., Berndt, F., Gruber, M., Linder, J. U., Truffault, V., Schultz, A., Martin, J., Schultz, J. E., Lupas, A. N., and Coles, M. (2006) The HAMP domain structure implies helix rotation in transmembrane signaling. *Cell 126*, 929−940.
(31) Buron-Barral, M. D., Gosink, K. K., and Parkinson, J. S. (2006) Loss- and gain-of-function mutations in the F1-HAMP region of the *Escherichia coli* aerotaxis transducer Aer. *J. Bacteriol. 188*, 3477−3486.
(32) Mehan, R. S., White, N. C., and Falke, J. J. (2003) Mapping out regions on the surface of the aspartate receptor that are essential for kinase activation. *Biochemistry 42*, 2952−2959.
(33) Kim, K. K., Yokota, H., and Kim, S. H. (1999) Four-helical-bundle structure of the cytoplasmic domain of a serine chemotaxis receptor. *Nature 400*, 787−792.
(34) Park, S. Y., Borbat, P. P., Gonzalez-Bonet, G., Bhatnagar, J., Freed, J. H., Bilwes, A. M., and Crane, B. R. (2006) Reconstruction of the chemotaxis receptor:kinase assembly. *Nat. Struct. Mol. Biol. 13*, 400−407.
(35) Pollard, A. M., Bilwes, A. M., and Crane, B. R. (2009) The Structure of a Soluble Chemoreceptor Suggests a Mechanism for Propagating Conformational Signals. *Biochemistry 48*, 1936−1944.
(36) Borkovich, K. A., Alex, L. A., and Simon, M. I. (1992) Attenuation of sensory receptor signaling by covalent modification. *Proc. Natl. Acad. Sci. U. S. A. 89*, 6756−6760.
(37) Li, G., and Weis, R. M. (2000) Covalent modification regulates ligand binding to receptor complexes in the chemosensory system of *Escherichia coli*. *Cell 100*, 357−365.
(38) Bornhorst, J. A., and Falke, J. J. (2000) Attractant regulation of the aspartate receptor-kinase complex: Limited cooperative interactions between receptors and effects of the receptor modification state. *Biochemistry 39*, 9486−9493.
(39) Chao, X., Muff, T. J., Park, S. Y., Zhang, S., Pollard, A. M., Ordal, G. W., Bilwes, A. M., and Crane, B. R. (2006) A receptor-modifying deamidase in complex with a signaling phosphatase reveals reciprocal regulation. *Cell 124*, 561−571.
(40) Hess, J. F., Bourret, R. B., and Simon, M. I. (1988) Histidine phosphorylation and phosphoryl group transfer in bacterial chemotaxis. *Nature 336*, 139−143.
(41) Kofoid, E. C., and Parkinson, J. S. (1988) Transmitter and receiver modules in bacterial signaling proteins. *Proc. Natl. Acad. Sci. U. S. A. 85*, 4981−4985.
(42) Alex, L. A., and Simon, M. I. (1994) Protein histidine kinases and signal transduction in prokaryotes and eukaryotes. *Trends Genet. 10*, 133−138.
(43) Bilwes, A. M., Alex, L. A., Crane, B. R., and Simon, M. I. (1999) Structure of CheA, a signal-transducing histidine kinase. *Cell 96*, 131−141.
(44) Welch, M., Chinardet, N., Mourey, L., Birck, C., and Samama, J. P. (1998) Structure of the CheY-binding domain of histidine kinase CheA in complex with CheY. *Nat. Struct. Biol. 5*, 25−29.
(45) Mourey, L., Da Re, S., Pedelacq, J. D., Tolstykh, T., Faurie, C., Guillet, V., Stock, J. B., and Samama, J. P. (2001) Crystal structure of the CheA histidine phosphotransfer domain that mediates response regulator phosphorylation in bacterial chemotaxis. *J. Biol. Chem. 276*, 31074−31082.
(46) Quezada, C. M., Gradinaru, C., Simon, M. I., Bilwes, A. M., and Crane, B. R. (2004) Helical shifts generate two distinct conformers in the atomic resolution structure of the CheA phosphotransferase domain from *Thermotoga maritima*. *J. Mol. Biol. 341*, 1283−1294.
(47) McEvoy, M. M., Muhandiram, D. R., Kay, L. E., and Dahlquist, F. W. (1996) Structure and dynamics of a CheY-binding domain of the chemotaxis kinase CheA determined by nuclear magnetic resonance spectroscopy. *Biochemistry 35*, 5633−5640.
(48) Park, S. Y., Beel, B. D., Simon, M. I., Bilwes, A. M., and Crane, B. R. (2004) In different organisms, the mode of interaction between two signaling proteins is not necessarily conserved. *Proc. Natl. Acad. Sci. U. S. A. 101*, 11646−11651.
(49) Wuichet, K., Alexander, R. P., and Zhulin, I. B. (2007) Comparative genomic and protein sequence analyses of a complex system controlling bacterial chemotaxis. *Methods Enzymol. 422*, 3−31.
(50) Sanders, D. A., Mendez, B., and Koshland, D. E. J. (1989) Role of the CheW protein in bacterial chemotaxis: overexpression is equivalent to absence. *J. Bacteriol. 171*, 6271−6278.
(51) Gegner, J. A., and Dahlquist, F. W. (1991) Signal transduction in bacteria: CheW forms a reversible complex with the protein kinase CheA. *Proc. Natl. Acad. Sci. U. S. A. 88*, 750−754.
(52) Griswold, I. J., Zhou, H., Matison, M., Swanson, R. V., McIntosh, L. P., Simon, M. I., and Dahlquist, F. W. (2002) The solution structure and interactions of CheW from *Thermotoga maritima*. *Nat. Struct. Biol. 9*, 567−568.
(53) Hamel, D. J., and Dahlquist, F. W. (2005) The contact interface of a 120 kD CheA-CheW complex by methyl TROSY interaction spectroscopy. *J. Am. Chem. Soc. 127*, 9676−9677.
(54) Miller, A. S., Kohout, S. C., Gilman, K. A., and Falke, J. J. (2006) CheA kinase of bacterial chemotaxis: Chemical mapping of four essential docking sites. *Biochemistry 45*, 8699−8711.
(55) Zhao, J. S., and Parkinson, J. S. (2006) Cysteine-scanning analysis of the chemoreceptor-coupling domain of the Escherichia coli chemotaxis signaling kinase CheA. *J. Bacteriol. 188*, 4321−4330.
(56) Zhao, J. H., and Parkinson, J. S. (2006) Mutational analysis of the chemoreceptor-coupling domain of the Escherichia coli chemotaxis signaling kinase CheA. *J. Bacteriol. 188*, 3299−3307.
(57) Ames, P., and Parkinson, J. S. (1994) Constitutively signaling fragments of Tsr, the *E.coli* serine chemoreceptor. *J. Bacteriol. 176*, 6340−6348.
(58) Borkovich, K. A., Kaplan, N., Hess, J. F., and Simon, M. I. (1989) Transmembrane signal transduction in bacterial chemotaxis involves ligand-depenent activation of phosphate group transfer. *Proc. Natl. Acad. Sci. U. S. A. 86*, 1208−1212.
(59) Asinas, A. E., and Weis, R. M. (2006) Competitive and cooperative interactions in receptor signaling complexes. *J. Biol. Chem. 281*, 30512−30523.
(60) Cardozo, M. J., Massazza, D. A., Parkinson, J. S., and Studdert, C. A. (2010) Disruption of chemoreceptor signalling arrays by high levels of CheW, the receptor-kinase coupling protein. *Mol. Microbiol. 75*, 1171−1181.
(61) Bhatnagar, J., Borbat, P., Pollard, A. M., Bilwes, A. M., Freed, J. R., and Crane, B. R. (2010) Structure of the ternary complex formed by a chemotaxis receptor signaling domain, the CheA histidine kinase and

the coupling protein CheW as determined by pulsed dipolar ESR spectroscopy. *Biochemistry 49*, 3824−3841.
(62) Briegel, A. L., X. Bilwes, A. M., Hughes, K. T., Jensen, G., and Crane, B. R. (2012) Bacterial chemoreceptor arrays are hexagonally packed trimers of receptor dimers networked by rings of kinase and coupling proteins. *Proc. Natl. Acad. Sci. U. S. A. 109*, 3766−3771.
(63) Vu, A., Wang, X., Zhou, H., and Dahlquist, F. W. (2012) The Receptor-CheW Binding Interface in Bacterial Chemotaxis. *J. Mol. Biol. 415*, 759−767.
(64) Wang, X. Q., Vu, A., Lee, K., and Dahlquist, F. W. (2012) CheA-Receptor Interaction Sites in Bacterial Chemotaxis. *J. Mol. Biol. 422*, 282−290.
(65) Piasta, K. N., Ullimann, C. J., Slivka, P. F., and Falke, J. J. (2013) Elucidating Receptor-CheA Kinase Contacts in the Membrane-Bound Chemosensory Array of Bacteria using Disulfide Mapping and TAM-IDS. *Biochemistry*, DOI: 10.1021/bi400385c.
(66) Otwinowski, A., and Minor, W. (1997) Processing of X-ray diffraction data in oscillation mode. *Methods Enzymol. 276*, 307−325.
(67) McCoy, A. J., Grosse-Kunstleve, R. W., Adams, P. D., Winn, M. D., Storoni, L. C., and Read, R. J. (2007) Phaser crystallographic software. *J. Appl. Crystallogr. 40*, 658−674.
(68) McRee, D. E. (1999) XtalView Xfit - A versatile program for manipulating atomic coordinates and electron density. *J. Struct. Biol. 125*, 156−165.
(69) Adams, P. D., Afonine, P. V., Bunkoczi, G., Chen, V. B., Echols, N., Headd, J. J., Hung, L. W., Jain, S., Kapral, G. J., Kunstleve, R. W. G., McCoy, A. J., Moriarty, N. W., Oeffner, R. D., Read, R. J., Richardson, D. C., Richardson, J. S., Terwilliger, T. C., and Zwart, P. H. (2011) The Phenix software for automated determination of macromolecular structures. *Methods 55*, 94−106.
(70) Su, J., Li, Y., Shaw, N., Zhou, W. H., Zhang, M., Xu, H., Wang, B. C., and Liu, Z. J. (2010) Crystal structure of a novel non-Pfam protein PF2046 solved using low resolution B-factor sharpening and multi-crystal averaging methods. *Protein Cell 1*, 453−458.
(71) Ulrich, L. E., and Zhulin, I. B. (2010) The MiST2 database: a comprehensive genomics resource on microbial signal transduction. *Nucleic Acids Res. 38*, D401−407.
(72) Altschul, S. F., Madden, T. L., Schaffer, A. A., Zhang, J., Zhang, Z., Miller, W., and Lipman, D. J. (1997) Gapped BLAST and PSI-BLAST: a new generation of protein database search programs. *Nucleic Acids Res. 25*, 3389−3402.
(73) Katoh, K., and Toh, H. (2010) Parallelization of the MAFFT multiple sequence alignment program. *Bioinformatics 26*, 1899−1900.
(74) Waterhouse, A. M., Procter, J. B., Martin, D. M., Clamp, M., and Barton, G. J. (2009) Jalview Version 2–a multiple sequence alignment editor and analysis workbench. *Bioinformatics 25*, 1189−1191.
(75) Tamura, K., Peterson, D., Peterson, N., Stecher, G., Nei, M., and Kumar, S. (2011) MEGA5: molecular evolutionary genetics analysis using maximum likelihood, evolutionary distance, and maximum parsimony methods. *Mol. Biol. Evol. 28*, 2731−2739.
(76) Moreno-Hagelsieb, G., and Collado-Vides, J. (2002) A powerful non-homology method for the prediction of operons in prokaryotes. *Bioinformatics 18* (Suppl 1), S329−336.
(77) da Silveira, C. H., Pires, D. E., Minardi, R. C., Ribeiro, C., Veloso, C. J., Lopes, J. C., Meira, W., Jr., Neshich, G., Ramos, C. H., Habesch, R., and Santoro, M. M. (2009) Protein cutoff scanning: A comparative analysis of cutoff dependent and cutoff free methods for prospecting contacts in proteins. *Proteins 74*, 727−743.
(78) Park, S. Y., Quezada, C. M., Bilwes, A. M., and Crane, B. R. (2004) Subunit exchange by CheA histidine kinases from the mesophile *Escherichia coli* and the thermophile thermotoga maritima. *Biochemistry 43*, 2228−2240.
(79) Berggard, T., Linse, S., and James, P. (2007) Methods for the detection and analysis of protein-protein interactions. *Proteomics 7*, 2833−2842.
(80) Gosink, K. K., Zhao, Y. M., and Parkinson, J. S. (2011) Mutational Analysis of N381, a Key Trimer Contact Residue in Tsr, the *Escherichia coli* Serine Chemoreceptor. *J. Bacteriol. 193*, 6452−6460.
(81) Mowery, P., Ostler, J. B., and Parkinson, J. S. (2008) Different Signaling Roles of Two Conserved Residues in the Cytoplasmic Hairpin Tip of Tsr, the *Escherichia coli* Serine Chemoreceptor. *J. Bacteriol. 190*, 8065−8074.
(82) Boukhvalova, M., Dahlquist, F. W., and Stewart, R. C. (2002) CheW binding interactions with CheA and Tar - Importance for chemotaxis signaling in *Escherichia coli*. *J. Biol. Chem. 277*, 22251−22259.
(83) Boukhvalova, M., VanBruggen, R., and Stewart, R. C. (2002) CheA kinase and chemoreceptor interactions on CheW. *J. Biol. Chem. 277*, 23596−23603.
(84) Liu, J. D., and Parkinson, J. S. (1991) Genetic evidence for interaction between the CheW and Tsr proteins during chemoreceptor signaling by *Escherichia coli*. *J. Bacteriol. 173*, 4941−4951.
(85) Pazos, F., and Valencia, A. (2008) Protein co-evolution, co-adaptation and interactions. *EMBO J. 27*, 2648−2655.
(86) Wuichet, K., and Zhulin, I. B. (2010) Origins and diversification of a complex signal transduction system in prokaryotes. *Sci. Signal. 3*, ra50.
(87) Weigt, M., White, R. A., Szurmant, H., Hoch, J. A., and Hwa, T. (2009) Identification of direct residue contacts in protein-protein interaction by message passing. *Proc. Natl. Acad. Sci. U. S. A. 106*, 67−72.
(88) Lybarger, S. R., Nair, U., Lilly, A. A., Hazelbauer, G. L., and Maddock, J. R. (2005) Clustering requires modified methyl-accepting sites in low-abundance but not high-abundance chemoreceptors of *Escherichia coli*. *Mol. Microbiol. 56*, 1078−1086.
(89) Porter, S. L., Wadhams, G. H., and Armitage, J. P. (2008) Rhodobacter sphaeroides: complexity in chemotactic signalling. *Trends Microbiol. 16*, 251−260.
(90) Bardy, S. L., and Maddock, J. R. (2005) Polar localization of a soluble methyl-accepting protein of Pseudomonas aeruginosa. *J. Bacteriol. 187*, 7840−7844.
(91) Wadhams, G. H., Martin, A. C., Porter, S. L., Maddock, J. R., Mantotta, J. C., King, H. M., and Armitage, J. P. (2002) TlpC, a novel chemotaxis protein in Rhodobacter sphaeroides, localizes to a discrete region in the cytoplasm. *Mol. Microbiol. 46*, 1211−1221.
(92) Watts, K. J., Taylor, B. L., and Johnson, M. S. (2011) PAS/poly-HAMP signalling in Aer-2, a soluble haem-based sensor. *Mol. Microbiol. 79*, 686−699.
(93) Collins, R. N., Holz, R. W., and Zimmerberg, J. (2012) The Biophysics of Membrane Fusion. *Compr. Biophys. 5*, 273−289.
(94) Rizo, J., Rosen, M. K., and Gardner, K. H. (2012) Enlightening molecular mechanisms through study of protein interactions. *J. Mol. Cell Biol. 4*, 270−283.
(95) Lamb, R. A., and Jardetzky, T. S. (2007) Structural basis of viral invasion: lessons from paramyxovirus F. *Curr. Opin. Struct. Biol. 17*, 427−436.
(96) Gibbons, D. L., Vaney, M. C., Roussel, A., Vigouroux, A., Reilly, B., Lepault, J., Kielian, M., and Rey, F. A. (2004) Conformational change and protein protein interactions of the fusion protein of Semliki Forest virus. *Nature 427*, 320−325.
(97) Igonet, S., Vaney, M. C., Vonhrein, C., Bricogne, G., Stura, E. A., Hengartner, H., Eschli, B., and Rey, F. A. (2011) X-ray structure of the arenavirus glycoprotein GP2 in its postfusion hairpin conformation. *Proc. Natl. Acad. Sci. U. S. A. 108*, 19967−19972.
(98) Luque, L. E., and Russell, C. J. (2007) Spring-loaded heptad repeat residues regulate the expression and activation of paramyxovirus fusion protein. *J. Virol. 81*, 3130−3141.
(99) Underbakke, E. S., Zhu, Y. M., and Kiessling, L. L. (2011) Protein footprinting in a complex milieu:identifying the interaction surfaces of the chemotaxis adaptor protein CheW. *J. Mol. Biol. 409*, 483−495.
(100) Levit, M. N., Grebe, T. W., and Stock, J. B. (2002) Organization of the receptor-kinase signaling array that regulates *Escherichia coli* chemotaxis. *J. Biol. Chem. 277*, 36748−36754.
(101) Wang, X. Q., Wu, C., Anh Vu, J. E. S., and Dahlquist, F. W. (2012) Computational and Experimental Analyses Reveal the Essential Roles of Interdomain Linkers in the Biological Function of Chemotaxis Histidine Kinase CheA. *J. Am. Chem. Soc. 134*, 16107−16110.